Geophysical Prospecting

EAGE EUROPEAN ASSOCIATION OF GEOSCIENTISTS & ENGINEERS

Geophysical Prospecting, 2015 doi: 10.1111/1365-2478.12263

Geophone-ground coupling with flat bases

José M. Carcione[1]*, Hashim S. Almalki[2] and Ayman N. Qadrouh[2,3]

[1]*Istituto Nazionale di Oceanografia e di Geofisica Sperimentale (OGS), Borgo Grotta Gigante 42c, 34010 Sgonico, Trieste, Italy,* [2]*SAC - KACST, PO Box 6086, Riyadh 11442, Saudi Arabia (E-mail: halmalki@kacst.edu.sa), and* [3]*Department of Geosciences, Faculty of Petroleum Technology, Universiti Teknologi Petronas, Bandar Seri Iskandar, 31750 Tronoh, Perak, Malaysia*

Received July 2014, revision accepted January 2015

ABSTRACT

Seismic acquisition can be costly and inefficient when using spiked geophones. In most cases, such as the desert, the most practical solution is the use of flat bases, where geophone-ground coupling is based on an optimal choice of the mass and area of contact between the receiver and the ground. This optimization is necessary since areas covered by sand are loose sediments and poor coupling occurs. Other cases include ground coupling in stiff pavements, for instance urban areas and ocean-bottom nodes. We consider three different approaches to analyse coupling and model the geophone with a flat base (plate) resting on an elastic half-space. Two existing models, based on the full-wave theory, which we refer to as the Wolf and Hoover-O'Brien models, predict a different behaviour with respect to the novel method introduced in this work. This method is based on the transmission coefficient of upgoing waves impinging in the geophone-ground contact, where the ground is described as an anelastic half-space. The boundary conditions at the contact have already been used to model fractures and are shown here to provide the equation of the damped oscillator. This fracture-contact model depends on the stiffness characteristic of the contact between the geophone base plate and the ground. The transmission coefficient from the ground to the plate increases for increasing weight and decreasing base plate area. The new model predicts that the resonant frequency is independent of the geophone weight and plate radius, while the recorded energy increases with increasing weight and decreasing base plate area (as shown from our own experiments and measurements by Krohn) which is contrary to the theories developed by Wolf and Hoover-O'Brien. The transient response is obtained by an inverse Fourier transform. Optimal geophone-ground coupling and energy transmission are required, the first concept meaning that the geophone is following the motion of the ground and the second one that the signal is detectable. As a final example, we simulate seismic acquisition based on the novel theory, showing the differences between optimal and poor ground-to-geophone energy transmission.

Key words: Geophone coupling, Transmission coefficient, Anelasticity, Resonant frequency.

INTRODUCTION

Seismic acquisition in the desert, where receivers have to be deployed over areas covered by sand, could be performed more efficiently with the use of land streamers, since the planting of spiked geophones is costly. Another situation where the use of flat bases is relevant in the deployment of ocean-bottom seismometers or 'ocean-bottom nodes' (Beaudoin and Reasnor 2010). The autonomous character of these devices facilitates good coupling with the sea-bed, unlike ocean-bottom cables,

*E-mail: jcarcione@inogs.it

where the coupling is affected by the tension in the cable. On the other hand, geophones mounted to iron base plates have been used with success on paved surfaces (Miller, Tsoflias and Steeples 2009).

Basically, coupling conditions can be defined on the basis of high-and low-resonance frequencies, respectively. The optimal case occurs when the seismic frequency response has an amplitude near unity and a coupling phase lag near zero. In this frequency range the geophone response follows the ground motion. There have been a few works on the theory of geophone-ground coupling, starting from Wolf (1944), who obtained the equation of motion of the system (a damped oscillator) assuming a ground described by a Poisson medium. In the Wolf model, the geophone is represented by a cylinder placed on the surface of an elastic solid. The elastic restoring forces are determined by the area of contact between the weight and the surface of the solid and by the elastic moduli of the solid, while the damping force is due to emission of elastic waves by the oscillating weight. Later, Lamer (1970) and Hoover and O'Brien (1980) generalized Wolf's equation. These authors obtained an integral equation for the amplitude of the geophone motion, which depends on the geophone mass and radius of the base. As before, the damping results from the wave scattering at the base. The Hoover-O'Brien model establishes that a small mass with large bases produces high-resonant frequencies and relatively large damping, while a large mass with smaller bases has low-resonant frequencies and a smaller amount of damping. Krohn (1984) studied the geophone-ground system by using a phenomenological model, represented by a mass coupled to the ground by a Kelvin-Voigt mechanical model (a parallel connection of a spring and a dashpot) (see Hoover and O'Brien 1980). One of the main conclusions is that the resonant frequency is insensitive to changes in the mass or diameter of the geophones, which disagrees with the results of the Wolf and Hoover-O'Brien models. The resonant frequency depends mainly on the ground properties. Finally, Drijkoningen *et al.* (2006) introduced the effect of the spike, which does not apply here.

Land streamers have been used in snow covered areas (Eiken *et al.* 1989) and on roads and fields (van der Veen *et al.* 2001). It was found that land streamers can obtain comparable results to traditional spiked geophones (Dimech 2010). Moura and Senos Matias (2012) used coupling blocks made of several materials with a constant area of contact. They found that cement blocks with a weight of 7 kg yield comparable results to the spiked geophones, although it is clear from their Figs 9 and 10 that a weight of 1 kg performs equally well. One

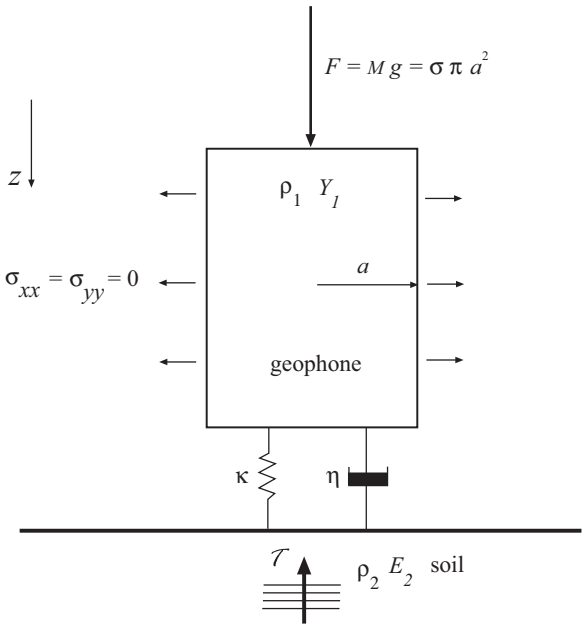

Figure 1 Geophone-ground coupling represented by a cylinder of radius a mass M, density ρ_1 and Young modulus Y_1 in contact with an elastic half-space of density ρ_2 and plane-wave modulus E_2. The lateral stresses vanish at the cylinder and the force acting on the contact is F, where g is the gravity constant. The boundary condition at the contact describes an imperfect bonding in terms of the specific normal stiffness κ and specific normal viscosity η. Optimum coupling is achieved when the energy transmission coefficient $\mathcal{T}$ of the upgoing waves is maximum.

of the challenges of designing a land streamer is to guarantee a desirable coupling of the geophone with the ground.

In this work, we investigate three approaches to analyse geophone-ground coupling. We first represent the system by using the Wolf and Hoover-O'Brien models (Models 1 and 2), which are based on a wave-theory approach and allow an explicit description of the system response as a function of the geophone and ground properties. We then develop Model 3, which is based on the transmission coefficient of the upgoing waves arriving at the geophone-ground interface, described by a displacement/particle-velocity boundary condition, already used to model wave propagation through fractures (Schoenberg 1980; Carcione 1996). The ground is modelled as a nearly-constant Q viscoelastic solid, based on continuum spectra of Zener mechanical models (e.g., Carcione 2007). The transmission coefficient can be cast in terms of the mass and area of the geophone, represented by a cylinder. We then derive the equation describing the motion (displacement) of the geophone, which corresponds to the classical damped harmonic oscillator. The equivalent mechanical model is the

Kelvin-Voigt viscoelastic solid (a parallel connection between a spring and a dashpot), where the parameters can be written in terms of the mass, area of the cylinder and stiffness characteristic of the contact between the base plate and ground. The last parameter can be obtained from data reported by Washburn and Wiley (1941).

MODELS BASED ON THE WAVE EQUATION

Two models are reported in the literature regarding flat bases (Wolf 1944; Hoover and O'Brien 1980). These models are based on the calculation of the full wavefield as wave scattering at the contact between the geophone and the ground. We consider a cylinder of radius a (the geophone) in contact with a homogeneous and isotropic half-space (the ground), as shown in Fig. 1. By simplicity, we denote the stress σ_{zz}, strain ϵ_{zz} and displacement u_z by σ, ϵ and u, respectively, such that $(\sigma_i, \epsilon_i, u_i)$, $i = 1,2$ denotes the field at the cylinder and ground, respectively and (x, y, z) is the position vector. The medium properties are indicated by ρ_i (mass density), v_i (wave velocity) λ_i and μ_i (Lamé constants), $E_i = \lambda_i + 2\mu_i$ and $Y_i = \mu_i(3\lambda_i + 2\mu_i)/(\lambda_i + \mu_i)$ (Young modulus). Moreover,

$$I_1 = \sqrt{\rho_1 Y_1}, \quad \text{and} \quad I_2 = \sqrt{\rho_2 E_2} \tag{1}$$

are characteristic impedances of the cylinder and ground, respectively, as we shall see below.

The Wolf theory (Model 1)

Wolf (1944) considered the following radial distribution of vertical stress on the base (see Fig. 1):

$$\begin{aligned} \sigma &= -\frac{F}{2\pi a\sqrt{a^2 - r^2}}, \quad \text{for} \quad r < a, \\ \sigma &= 0, \qquad\qquad\qquad \text{for} \quad r \geq a, \end{aligned} \tag{2}$$

where F is an harmonic force. This is then replaced by the inertia of the weight. Wolf (1944) assumed that the displacement of the weight is equal to the average displacement produced by the assumed distribution of stress on the surface of the solid. The equation of motion obtained by Wolf (1944) is an approximation, under the assumption of a Poisson lossless ground ($\lambda = \mu$) and to second-order in the displacement. It is:

$$(M + 0.82\rho_2 a^3)\ddot{u}_1 + 2.43 I_2 a^2 \dot{u}_1 + 1.778 a E_2 u_1 = 0, \tag{3}$$

where u_1 is the displacement averaged over the base of the cylinder and M is the mass of the cylinder. A dot above a variable denotes time differentiation.

Equation (3) holds for $M \gg \rho_2 a^3$ and has the oscillator form:

$$m\ddot{u}_1 + \eta\dot{u}_1 + \kappa u_1 = 0, \tag{4}$$

where m is mass per unit area, η is a viscosity per unit length and κ is a stiffness per unit length. In this case,

$$\begin{aligned} \kappa &= 1.778 a E_2, \\ \eta &= 2.43 I_2 a^2, \end{aligned} \tag{5}$$

and

$$\omega_0 \equiv \sqrt{\frac{\kappa}{m}} = 1.332\sqrt{\frac{a E_2}{M + 0.82\rho_2 a^3}} \tag{6}$$

and

$$\bar{\eta} \equiv \frac{\eta}{\sqrt{\kappa m}} = 1.822\sqrt{\frac{\rho_2 a^3}{M}} \tag{7}$$

are the resonance frequency and viscosity parameter respectively. This model can be useful to obtain the density and seismic velocity of the ground, knowing the resonant frequency $f_0 = \omega_0/(2\pi)$ and damping parameter $\bar{\eta}$. From equations (6) and (7) we obtain:

$$\rho_2 = \frac{\bar{\eta}^2 M}{3.32 a^3} \tag{8}$$

and

$$v_2 = \frac{8.66 a f_0}{\bar{\eta}}\sqrt{1 + 0.25\bar{\eta}^2}. \tag{9}$$

The Hoover-O'Brien theory (Model 2)

The theory developed by Hoover and O'Brien (1980) also considers an infinitely rigid geophone over an elastic half-space. The amplitude of the geophone motion is:

$$U = \left[1 + \frac{M\rho_2\omega^4}{\pi\mu_2^2 a}\int_0^\infty \frac{k_1 J_1(ak)}{R(k)} dk\right]^{-1}, \tag{10}$$

where ω is the angular frequency, k is the wavenumber, J_1 is the first-order Bessel function of the first kind,

$$R(k) = (2k^2 - k_S^2)^2 - 4k^2 k_1 k_2 \tag{11}$$

is the Rayleigh function and

$$\begin{aligned} k_1 &= \sqrt{k^2 - k_P^2}, \qquad k > k_P, \quad k_P^2 = \rho\omega^2/E_2 \\ &= \mathrm{i}\sqrt{k_P^2 - k^2}, \qquad k < k_P, \\ k_2 &= \sqrt{k^2 - k_S^2}, \qquad k > k_S, \quad k_S^2 = \rho\omega^2/\mu_2 \\ &= \mathrm{i}\sqrt{k_S^2 - k^2} \qquad k < k_S. \end{aligned} \tag{12}$$

Equation (10) is solved in the appendix by using a different method as that of Hoover and O'Brien (1980). Equation (6) (the Wolf model) indicates that the resonant frequency increases with increasing plate radius (for $M \gg \rho_2 a^3$). The same property is predicted by the theory developed by Hoover and O'Brien (1980). The novel model presented in the next section predicts a constant resonance frequency.

MODEL 3

Model 3 is introduced in this work. It is based on a boundary condition used to describe fractures and involves the transmission coefficient of the upgoing seismic waves impinging in the geophone-ground contact.

Stress-strain relations

Referring to Fig. 1, ignoring shear stresses and shear deformations, the stress-strain relation can be written as:

$$\begin{aligned} \sigma_{xx} &= E\epsilon_{xx} + \lambda(\epsilon_{yy} + \epsilon_{zz}),\\ \sigma_{yy} &= E\epsilon_{yy} + \lambda(\epsilon_{xx} + \epsilon_{zz}),\\ \sigma_{zz} &= E\epsilon_{zz} + \lambda(\epsilon_{xx} + \epsilon_{yy}) \end{aligned} \tag{13}$$

(e.g., Carcione 2007), where:

$$\epsilon_{xx} = \partial_x u_x, \quad \epsilon_{yy} = \partial_y u_y, \quad \epsilon_{zz} = \partial_z u_z, \tag{14}$$

with (u_x, u_y, u_z) being the displacement vector. The symbol ∂ indicates spatial partial differentiation.

The cylinder is laterally free implying $\sigma_{xx} = \sigma_{yy} = 0$. By symmetry $\epsilon_{xx} = \epsilon_{yy}$ and therefore $\epsilon_{xx} = -[\lambda_1/(E_1 + \lambda_1)]\epsilon_{zz}$ from equation (13). Since $\sigma_{zz} = E_1\epsilon_{zz} + 2\lambda_1\epsilon_{xx}$, we obtain:

$$\sigma_{zz} = Y_1\epsilon_{zz}. \tag{15}$$

We assume $\epsilon_{xx} = \epsilon_{yy} = 0$ under the effect of the weight of the cylinder, meaning that the medium surrounding the ground under the cylinder generates a reaction stress, compensating possible motions along the horizontal direction. Hence

$$\sigma_{zz} = E_2\epsilon_{zz}, \tag{16}$$

in the ground.

Since we consider unconsolidated grounds, such as areas covered by sand, wave attenuation can be significant. We replace:

$$E_2 \to E_2(1 + \mathrm{i}Q^{-1}) \tag{17}$$

where Q is the quality factor, which is assumed to be constant with frequency and $\mathrm{i} = \sqrt{-1}$. The medium is therefore represented by an anelastic half-space.

Boundary conditions

The boundary conditions at the base of the cylinder/ground interface depend on the weight of the cylinder and spans from lack of bonding at zero weight to perfect (welded) bonding at infinite weight. This effect can be modelled by the displacement/particle-velocity discontinuity boundary condition:

$$\begin{aligned} \kappa[u_z] + \eta[\dot{u}_z] &= \sigma_{zz},\\ [\sigma_{zz}] &= 0, \end{aligned} \tag{18}$$

where $\dot{u}_z$ is the particle velocity and κ and η are the specific normal stiffnesses and normal viscosity, which have dimensions of stiffness and viscosity per unit length, respectively. The brackets denote discontinuities across the interface, such that for a field variable ϕ, it is $[\phi] = \phi_2 - \phi_1$, where '1' refers to the cylinder and '2' to the ground. In the frequency domain, equation (18) involves the complex stiffness $\kappa + \mathrm{i}\omega\eta$, where ω is the angular frequency. There is energy loss at the interface and corresponds to the damped oscillator as we shall see later. This model was used by Carcione (1996, 1998, 2007) and Carcione and Picotti (2012) to obtain the reflection and transmission coefficients of fractures and cracks.

Experimental values of κ for fractures can be found, for instance, in Pyrak-Nolte, Xu and Haley (1992). The material is aluminium and the experiments were performed at a frequency of 1 MHz. Normal stresses between 0–30 MPa imply values of κ from 7–30 GPa/mm, approximately. Fioravante *et al.* (1999) performed tests on sand-aluminium contacts under varying normal stress. A typical value for Toyoura sand is 1 MPa/mm for a normal stress of 50 kPa (equivalent to a weight of 392 kg at the Earth's surface). In general the κ values in this work range from 0–100 kPa/mm.

Reflection and transmission coefficient

Using compact notation, the stress-strain relations (15) and (16) and boundary condition (18) read:

$$\begin{aligned} \sigma_1 &= Y_1\epsilon_1,\\ \sigma_2 &= E_2\epsilon_2,\\ \kappa(u_2 - u_1) &= \sigma_1 = \sigma_2 = \sigma, \end{aligned} \tag{19}$$

where we assumed $\eta = 0$. Let us consider the plane-wave solution with an incident wave on the cylinder coming from the soil,

$$\begin{aligned} u_1 &= T\exp[\mathrm{i}(\omega t + k_1 z)], \\ u_2 &= \exp[\mathrm{i}(\omega t + k_2 z)] + R\exp[\mathrm{i}(\omega t - k_2 z)], \end{aligned} \tag{20}$$

where t is the time variable, R and T are the reflection and transmission coefficients, and

$$k_1 = \frac{\omega}{v_1}, \quad \text{and} \quad k_2 = \frac{\omega}{v_2} \tag{21}$$

are the wavenumbers, with

$$v_1 = \sqrt{\frac{Y_1}{\rho_1}} \quad \text{and} \quad v_2 = \sqrt{\frac{E_2}{\rho_2}} \tag{22}$$

the wave velocities.

From equation (14) we have at $z = 0$,

$$\begin{aligned} \epsilon_1 &= \mathrm{i}k_1 T\exp(\mathrm{i}\omega t), \\ \epsilon_2 &= \mathrm{i}k_2(1 - R)\exp(\mathrm{i}\omega t), \end{aligned} \tag{23}$$

and equation (19) gives:

$$\begin{aligned} \sigma_1 &= \mathrm{i}k_1 Y_1 T\exp(\mathrm{i}\omega t), \\ \sigma_2 &= \mathrm{i}k_2 E_2(1 - R)\exp(\mathrm{i}\omega t). \end{aligned} \tag{24}$$

The third boundary condition (19) yields two equations with the two unknowns R and T,

$$\begin{aligned} \kappa(1 + R - T) &= \mathrm{i}I_1\omega T, \\ I_1 T &= I_2(1 - R), \end{aligned} \tag{25}$$

where I_1 and I_2 are defined in equation (1). The solution is:

$$\begin{aligned} R &= \frac{I_2 - I_1 + \mathrm{i}\gamma}{I_1 + I_2 + \mathrm{i}\gamma}, \quad \gamma = \frac{\omega I_1 I_2}{\kappa}, \\ T &= \frac{2I_2}{I_1 + I_2 + \mathrm{i}\gamma}. \end{aligned} \tag{26}$$

The welded interface is obtained for $\kappa \to \infty$ ($\gamma \cdot 0$) and the uncoupled case for $\kappa \to 0$ ($\gamma \cdot \infty$), for which $R = 1$ and $T = 0$. In the case of a particle-velocity discontinuity also, κ should be replaced with $\kappa + \mathrm{i}\omega\eta$ in equation (26).

The transmission coefficient is an amplitude scale factor, which varies slowly at low frequencies. Keeping constant the stiffness κ of the interface ground-plate, the transmission coefficient is $2I_2/(I_1 + I_2)$ at $\omega = 0$ and zero at high frequencies. Maximum transmission at $\omega = 0$ occurs when the plate and the ground have the same properties. In this case, $T = 2/(1 + \sqrt{E/Y}) = 2/(1 + \sqrt{6/5}) \approx 0.95$ for a Poisson medium ($\lambda = \mu$).

Specific normal stiffness and energy transmission coefficient

Empirical models used for fractures relate the specific normal stiffness to the closure of a joint, c (Jiang *et al.* 2009). Normal stiffness and normal stress are related by:

$$\kappa = -\frac{d\sigma}{dc}, \tag{27}$$

with

$$c = c_0 - \frac{1}{b}\ln\left(\frac{\sigma}{\sigma_0}\right), \tag{28}$$

where c_0 is the aperture (or gap between the two sides of a joint) at a reference normal stress σ_0 and b is a fitting parameter that implicitly contains the properties of the medium. This parameter was termed 'stiffness characteristic' by Zangerl *et al.* (2008) and is indicated as $dk_n/d\sigma_n'$ in their paper. For instance, Zangerl *et al.* (2008) reported 57 1/mm for Pinawa granite, 68-141 1/mm for Dolerite and 25-113 1/mm for granite gneiss. Here, we obtain values from experimental data in the range [13,1050] 1/mm. Particularly, since b can be obtained from experiments, this parameter can be appropriate to model the joint properties between the plate and the soil solely based on physics.

We obtain from equations (27) and (28),

$$\kappa = b\sigma, \tag{29}$$

showing that the curve of normal stiffness versus normal stress is linear and passes through the origin (i.e., zero stiffness at zero normal stress) (Zangerl *et al.* 2008). Since the normal stress is:

$$\sigma = \frac{P}{\pi a^2} = \frac{Mg}{\pi a^2} = mg, \quad m = \frac{M}{\pi a^2}, \tag{30}$$

where P is the weight of the cylinder, m is mass per unit area and $g = 9.81$ m/s^2, we have:

$$\kappa = \frac{bP}{\pi a^2} = bmg. \tag{31}$$

Therefore, the stiffness is proportional to the cylinder mass and inversely proportional to its radius squared. We note here that weight P is actually a force given in newtons in the SI system, i.e, it is the weight at the surface of the Earth. However, we indicate P in kilograms, since this is common use, although it is not strictly correct.

We consider the energy transmission coefficient:

$$\mathcal{T} = \frac{I_1}{\mathrm{Re}(I_2)}|T|^2 = \frac{4I_1|I_2|^2}{\mathrm{Re}(I_2)[I_1 + \mathrm{Re}(I_2)]^2 + [\gamma + \mathrm{Im}(I_2)]^2} \tag{32}$$

(e.g., Pilant 1979; Carcione 2007), such that $|R|^2 + \mathcal{T} \approx 1$, where we have used equation (26); 'Re' and 'Im' take real and imaginary parts, respectively.

The damped oscillator

A wave equation of the form (4) can easily be obtained for the system shown in Fig. 1. Newton's second law $P = \pi a^2 \sigma = M\ddot{u}_1$, combined with the displacement/particle-velocity boundary condition:

$$\kappa(u_2 - u_1) + \eta(\dot{u}_2 - \dot{u}_1) = \sigma, \tag{33}$$

(see Fig. 1) yields:

$$m\ddot{u}_1 + \eta\dot{u}_1 + \kappa u_1 = \eta\dot{u}_2 + \kappa u_2. \tag{34}$$

Assuming a harmonic ground oscillation with unit amplitude:

$$u_2 = \exp(\mathrm{i}\omega t), \tag{35}$$

we obtain the solution:

$$u_1 = U\exp(\mathrm{i}\omega t), \tag{36}$$

where U is the amplitude at the geophone. Its expression is the geophone-ground coupling response, which is given by:

$$U = \frac{1 + \mathrm{i}(\omega/\omega_0)\bar{\eta}}{1 - (\omega/\omega_0)^2 + \mathrm{i}(\omega/\omega_0)\bar{\eta}}, \tag{37}$$

where ω_0 and $\bar{\eta}$ are defined in equations (6) and (7), respectively. In this case,

$$\omega_0 = \sqrt{bg} \quad \text{and} \quad \bar{\eta} = \frac{\pi a^2 \eta}{\omega_0 M}, \tag{38}$$

using equation (31). The undamped resonant frequency ω_0 is constant, in agreement with Krohn (1984), who concluded that there is no change in the resonance frequency for differently sized bases. Moreover, the resonant frequency is independent of the mass. This disagrees with the theoretical predictions of Hoover and O'Brien (1980) but agrees with the experimental results of Krohn (1984) (her Fig. 12). She stated "In spite of the increase in resonant frequency in the past, neither Washburn and Wiley (1941) who measured the coupling for geophones of 11 to 27 lb, nor Fail, Grau and Lavergne (1962) who measured coupling for geophones of 300 to 500 g, saw much change with mass. It is possible that the resonant frequency is influenced by large changes in size and mass but is fairly insensitive to only doubling the mass." As mentioned above, the medium properties enter implicitly in the fitting parameter b (see Table 1 in Zangerl *et al.* 2008).

Equation (37) is the expression given by Hoover and O'Brien (1980), which has been derived here from the boundary condition used to model fractures and cracks (Schoenberg 1980; Carcione 1996). That equation (37) also describes the behaviour of Models 1 and 2 is not surprising but the parameters are different and this implies a different behaviour. The displacement amplitude $|U|$ and related phase determine the response of the geophone. Since the incident seismic-wave amplitude is unity, $|U| = 1$ and phase equal to zero indicates that the geophone is following exactly the motion of the ground. This is the optimal situation.

Table 1 Properties of different grounds (from Washburn and Wiley 1941).

Ground	f_p (Hz)	U_p	f_0 (Hz)	f_0' (Hz)	κ (kPa/mm)	$\bar{\eta}$	b (1/mm)
Pure dry sand	130	2	140	133	43.4	0.60	78.6
Dry black gumbo	125	1.7	139	129	42.9	0.76	77.6
Dry sand clay (plowed)	67	2.9	69	68	10.6	0.37	19.2
Hard grassy ground	200	3.1	205	202	93.8	0.34	169.8
Dry sand clay loam	110	2.5	115	112	29.3	0.44	53
Damp sticky gumbo (plowed)	80	1.6	91	82	18.2	0.85	33
Wet sandy mud	70	2.2	74	71	12.2	0.52	22.1
Very wet sandy mud	56	3.2	57	56	7.3	0.33	13.3
Wet spongy loam	70	2.4	73	71	12	0.47	21.7
Asphalt road	470	1.9	509	482	576.7	0.64	1044

Notes: $a = 5.36$ cm; $P = 5$ kg.

The maximum amplitude, corresponding to equation (37), occurs at the frequency:

$$\omega_p = \frac{\omega_0}{\bar{\eta}}\sqrt{\sqrt{1 + 2\bar{\eta}^2} - 1}. \tag{39}$$

Its value is:

$$U_p = \frac{\bar{\eta}^2}{\sqrt{\bar{\eta}^4 + 2\left(\sqrt{1 + 2\bar{\eta}^2} - \bar{\eta}^2 - 1\right)}}. \tag{40}$$

Hence, from the experimental curve we can measure ω_p and U_p and obtain ω_0 and $\bar{\eta}$ from equations (39) and (40).

The transient response corresponding to equation (34) can be obtained by assuming an impulse in the ground of the form $u_2 = \delta(t)$, where δ is Dirac's function. The solution is given by the inverse Fourier transform,

$$u_1(t) = \mathcal{F}^{-1}[U(\omega)], \tag{41}$$

where U is given in equation (37). Using the Fourier-transform pairs:

$$\exp(-\alpha t)\sin(\omega_0' t)H(t) \Leftrightarrow \frac{\omega_0'}{{\omega_0'}^2 + (\alpha + \mathrm{i}\omega)^2},$$
$$\exp(-\alpha t)\cos(\omega_0' t)H(t) \Leftrightarrow \frac{\alpha + \mathrm{i}\omega}{{\omega_0'}^2 + (\alpha + \mathrm{i}\omega)^2}, \quad (42)$$

where H is the Heaviside function, we obtain:

$$u_1(t) = \left(\frac{\omega_0}{\omega_0'}\right)\left[\omega_0'\bar{\eta}\cos(\omega_0' t) + \omega_0\left(1 - \frac{\bar{\eta}^2}{2}\right)\sin(\omega_0' t)\right] \exp(-\bar{\eta}\omega_0 t/2)H(t), \quad (43)$$

where

$$\omega_0' = 2\pi f_0' = \omega_0\sqrt{1 - \bar{\eta}^2/4}, \quad (44)$$

assuming under-damped oscillations, i.e., $\bar{\eta} < 2$.

The internal mechanism of the geophone is also described as a damped oscillator and can be included in equation (37), which becomes:

$$U = \frac{(\omega/\omega_1)^2[1 + \mathrm{i}(\omega/\omega_0)\bar{\eta}]}{[1 - (\omega/\omega_1)^2 + \mathrm{i}(\omega/\omega_1)\bar{\eta}_1][1 - (\omega/\omega_0)^2 + \mathrm{i}(\omega/\omega_0)\bar{\eta}]}, \quad (45)$$

according to Krohn (1984), where ω_1 and $\bar{\eta}_1$ are the resonant frequency and damping parameter of the geophone.

RESULTS

Washburn and Wiley (1941) reported peak frequencies and peak amplitudes for several grounds corresponding to a geophone with a base area of 14 sq. in ($a = 5.36$ cm) and $P = 5$ kg (see their Table I). From Table I of Washburn and Wiley (1941), we obtain the normal stiffness as:

$$\kappa = m\omega_0^2 \quad (46)$$

and the viscosity from equation (40), where we used equations (6) and (39), based on equation (37). On the other hand, the stiffness characteristic can be obtained from equation (38),

$$b = \frac{\omega_0^2}{g}. \quad (47)$$

The values of the various quantities are reported in Table 1, where $\omega_p = 2\pi f_p$ and $\omega_0 = 2\pi f_0$.

We consider a geophone plate with $Y_1 = 200$ GPa and $\rho_1 = 7850$ kg/m^3 (steel) and a sandy ground with a P-wave velocity $v_2 = 200$ m/s and density $\rho_2 = 1700$ kg/m^3, such that $E_2 = \rho_2 v_2^2$ (Hunt and Vriend 2010). We first consider the Wolf model (Wolf 1944), given by equations (6), (38) and (45), i.e., including the geophone internal mechanism. The geophone

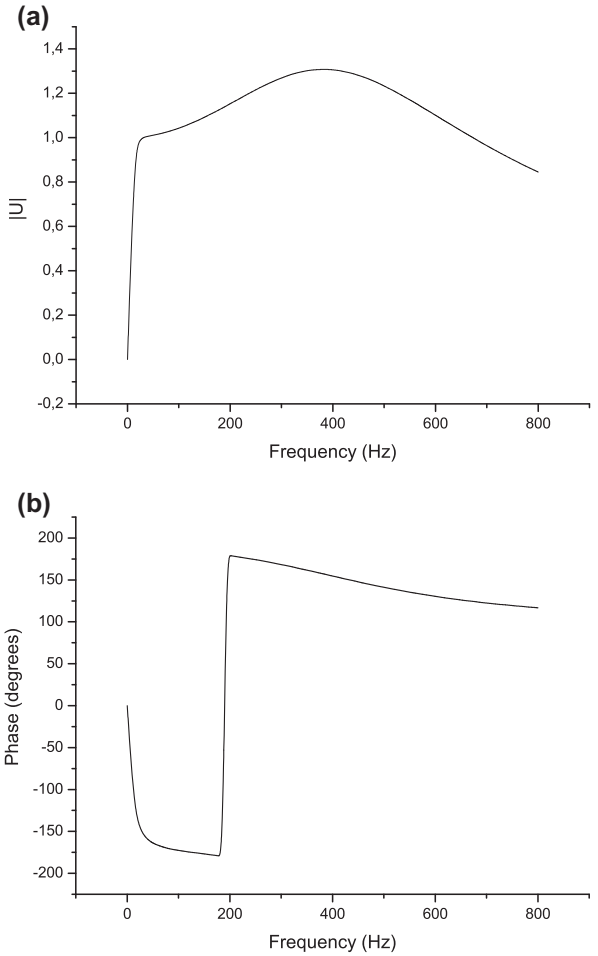

Figure 2 The Wolf theory (Wolf 1944) (Model 1). Geophone amplitude (a) and phase (b) as a function of frequency.

constants are $\bar{\eta}_1 = 1.4$ and $f_1 = 10$ Hz. Figure 2 shows the amplitude (a) and phase (b) for $a = 5.36$ cm and $P = 5$ kg, $\rho_2 = 1700$ kg/m^3, $v_2 = v_P = 200$ m/s and $v_S = v_P/\sqrt{3}$ (the Wolf model holds for a Poisson medium.) The model predicts $f_0 = 476$ Hz and $\bar{\eta} = 1.31$ for the sand properties assumed above. To obtain the resonant frequency and damping factor reported in the first row of Table 1 (pure dry sand), we have to use the ground properties $\rho_2 = 358$ kg/m^3 and $v_2 = 113$ m/s (see equations (8) and (9)). This model predicts a very low density for dry sand, whose value is in the range 1.6–1.7 g/cm^3. This is the reason why Wolf (1944) did not use equation (8) to predict the density. If we assume a density $\rho_2 = 1700$ kg/m^3, the velocity to match the resonant frequency is $v_2 = 59$ m/s but it does not match the damping factor $\bar{\eta}$ (we obtain a value of 1.3). The model of Hoover and O'Brien (1980) is compared to that of Wolf (1944) in Fig. 3. In this

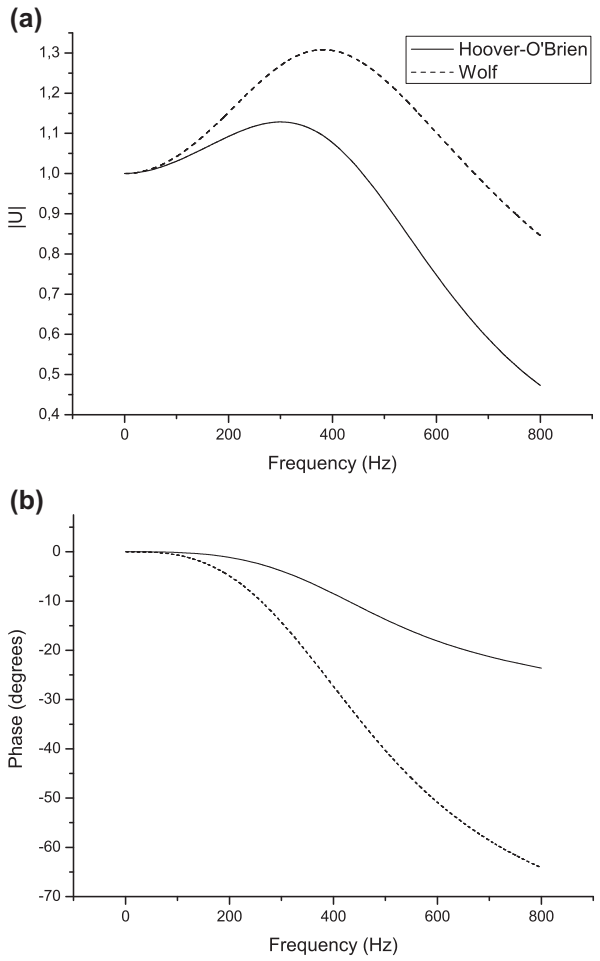

Figure 3 Geophone amplitude (a) and phase (b) as a function of frequency. Comparison between the Wolf (1944) and Hoover and O'Brien (1980) theories (Models 1 and 2, respectively), based on geophone characteristics reported in Washburn and Wiley (1941).

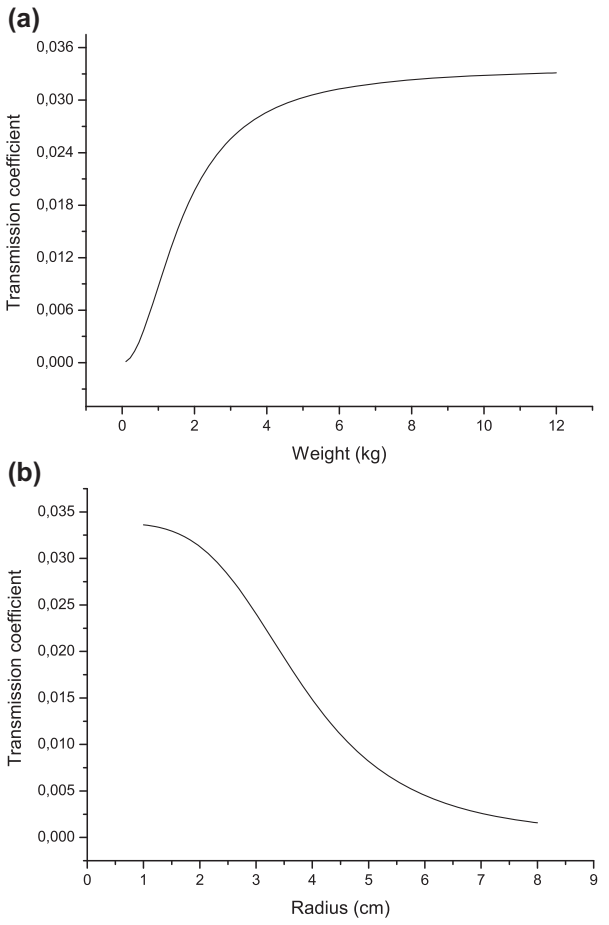

Figure 4 Model 3. Energy transmission coefficient as a function of weight (a) and radius (b). The frequency is 50 Hz. The geophone plate is made of steel.

case, we use equation (37) for Model 1, i.e., the geophone internal mechanism is not taken into account.

Let us now consider Model 3, where the attenuation parameter is assumed $Q = 10$. Moreover, $b = 78.6$ 1/mm for a sandy ground, according to Table 1. Figure 4 shows the energy transmission coefficient (32) as a function of weight (with $a = 2$ cm) (a) and radius (with $P = Mg = 6$ kg) (b) for $f = 50$ Hz. The values of κ range from 0.08–10 kPa/mm with varying weight (normal stress (weight/area) from 0.3–20 kPa) and from 20–1500 kPa/mm with varying radii (normal stress in the range 0.3 kPa–20 Pa) [see equation (31)]. In this particular case, the transmission coefficient increases with weight and decreases abruptly between 2–3 cm radii, with a maximum transmission of 3.5% at small areas. The best situation happens when the geophone plate has the same properties of the ground. In this case, $\rho_1 = \rho_2$ and $Y_1 = (5/6)\rho_2 v_2^2$, where we assumed a Poisson medium. The transmission coefficient is shown in Fig. 5, where we can see that 100% of the energy is transmitted. This model predicts more energy transmission for increasing weight and decreasing base plate area.

In the next example, we consider equation (45), with $a = 5.36$ cm, $b = 78.6$ 1/mm ($f_0 = 140$ Hz), $\bar{\eta} = 0.60$, $\bar{\eta}_1 = 1.4$ and $f_1 = \omega_1/(2\pi) = 10$ Hz. The amplitude and phase are shown in Fig. 6 (solid line). If $\bar{\eta} = 1$ (Krohn 1984), we have the dashed line. The viscosity parameter $\bar{\eta}$ has a significant influence in the amplitude. At the low-frequency limit, the geophone amplification is unity and the phase lag is zero, indicating a perfect coupling between the geophone and the ground. As frequency increases, the displacement becomes larger than the earth displacement and the geophone motion begins to lag the ground motion. As mentioned above, the resonant frequency of the

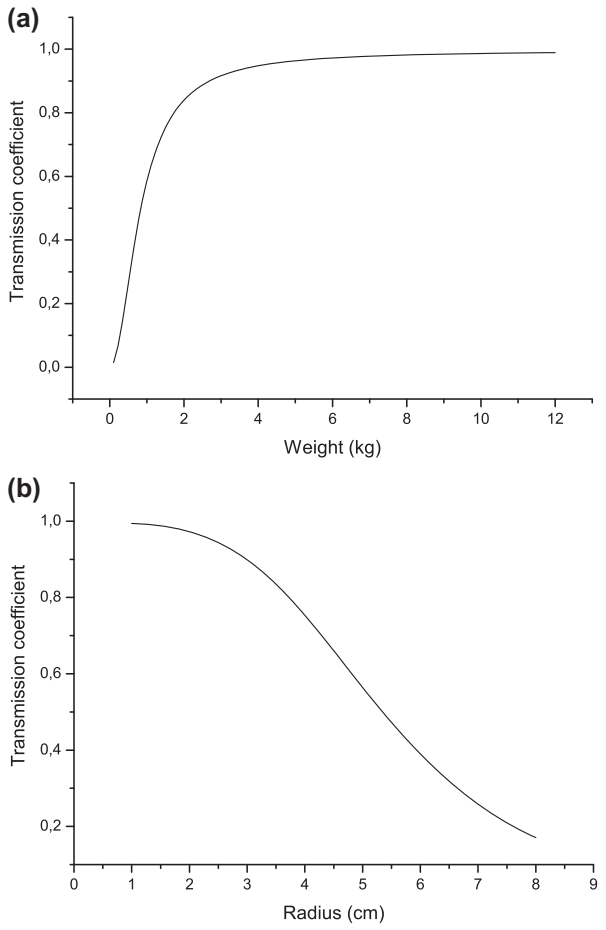

Figure 5 Model 3. Energy transmission coefficient as a function of weight (a) and radius (b). The frequency is 50 Hz. The geophone plate has the same properties of the ground.

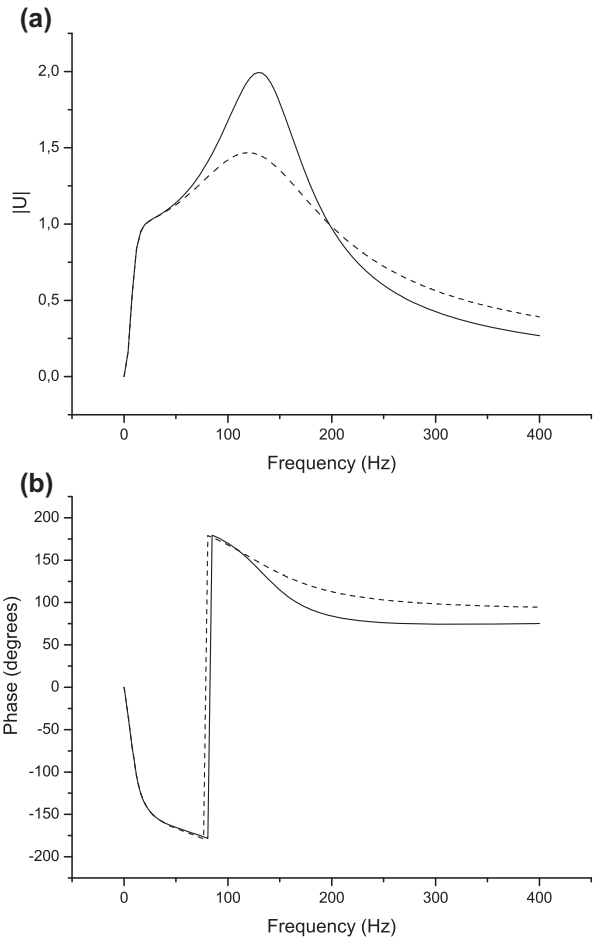

Figure 6 Model 3. Geophone amplitude for $\bar{\eta} = 0.6$ (solid line) and $\bar{\eta} = 1$ (dashed line). Moreover, $a = 5.36$ cm, $b = 78.6$ 1/mm, $\bar{\eta}_1 = 1.4$ and $f_1 = \omega_1/(2\pi) = 10$ Hz.

fracture model is independent of the weight and plate area [see equation (38)]. In Fig. 6, we consider the internal mechanism of the geophone, i.e., equation (45). On the other hand, without this effect (equation (37)) (see Fig. 7), the phase lag is approximately zero in a finite range of low frequencies till 100 Hz.

Geophone signals (43) for different grounds, corresponding to the fracture model, are shown in Fig. 8. The damping factor $\bar{\eta}$ and resonant frequency ω_0 were obtained from Table 1. Amplitude and resonant frequency increase as the ground becomes stiffer. As mentioned above, since the resonant frequency is independent of the plate weight and radius, the signal is the same for varying weight and radii.

Resonant frequencies obtained from laboratory experiments conducted at KACST are compared in Fig. 9 to the predictions of Model 3 and the Wolf model (Wolf 1944). In our experiments, we used the ELVIS hardware system and LabView software, which are tools for acquiring and processing digital signals. ELVIS is a device provided by National Instruments, containing a data-acquisition card as the fundamental core. We used a hammer as a source, whose strength is calibrated by letting it fall from a certain height and the geophones were manufactured by Geostuff. The stiffness characteristic b was used as a free parameter regarding Model 3. We considered $b = 3.16$/mm, $\rho_2 = 1700$ kg/m^3 and $E_2 = 1.7 \times 10^{-4}$ GPa. This low value of the P-wave modulus of the loose sand is used to scale the frequency values predicted by the Wolf model to the real values. Figure 9(a) shows the frequency as a function of the plate area. As can be appreciated, the frequency is constant and can be predicted by Model 3, while in this case the Wolf model predicts a decreasing frequency with increasing area of the plate. However, the results

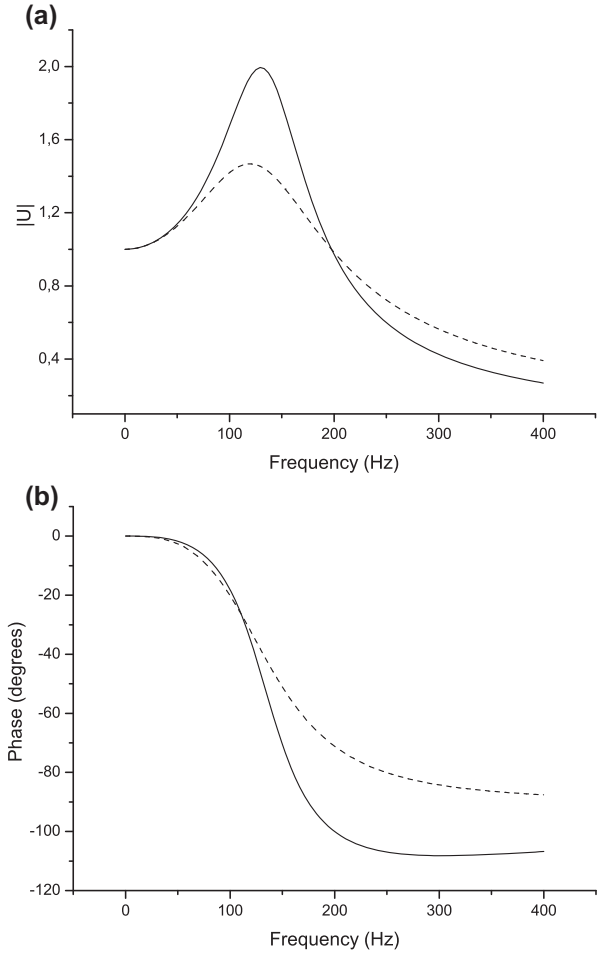

Figure 7 Model 3. Same as Fig. 6, without the geophone internal mechanism.

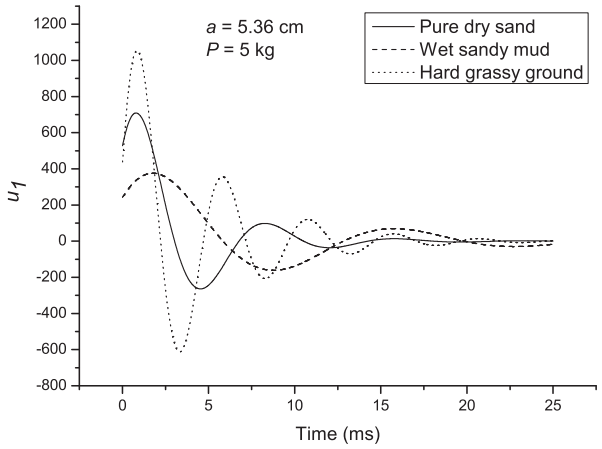

Figure 8 Model 3. Geophone signals (43) for different grounds and $a = 5.36$ cm and $P = 5$ kg.

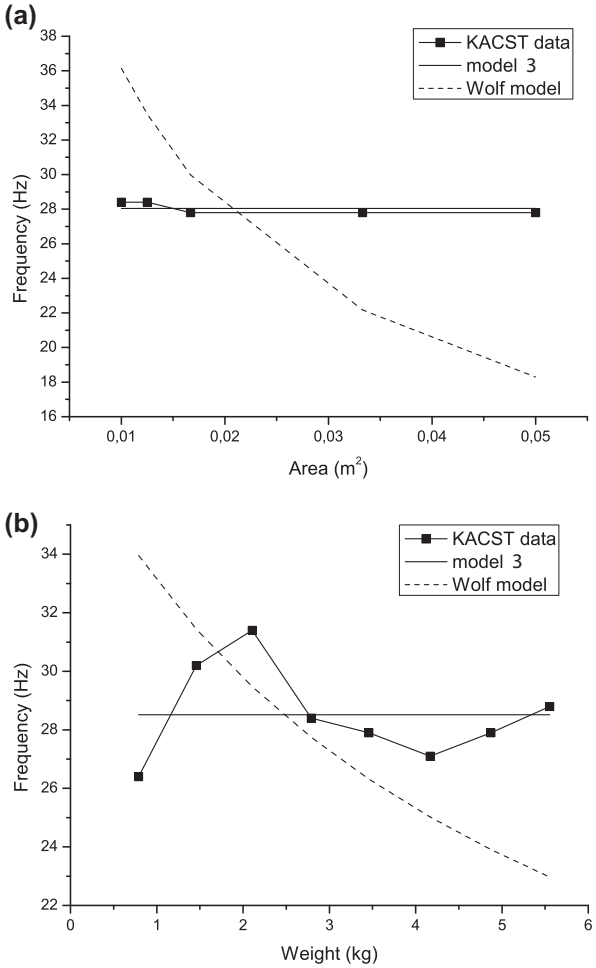

Figure 9 Resonant frequency as a function of the plate area (the weight is 0.78 kg) (a) and weight of the plate (the area is 120 cm^2) (b).

of the Wolf model have to be taken with caution since the condition $M \gg \rho_2 a^3$ is not satisfied. In this case, the opposite trend occurs in view of equation (6). On the other hand, Fig. 9(b) shows the frequency as a function of the weight of the plate. Similarly, the constancy of the frequency is the main trend while the Wolf model predicts a decreasing trend.

Finally, we simulate a seismic-acquisition experiment based on the geophone-ground coupling theory developed in this work, i.e., Model 3. The simulation algorithm, which considers P-and S-waves, can be found in Kosloff and Carcione (2010). We assume a vertical source with a central frequency of 70 Hz and 25 receivers at the surface. The model consists in a 1 m thickness surface sand layer with $v_P = 460$ m/s, $v_S = 200$ m/s, $\rho = 1722$ kg/m^3, $Q_P = 60$ and $Q_S = 50$, overlying a more consolidated layer with $v_P = 600$ m/s, $v_S = 346$ m/s,

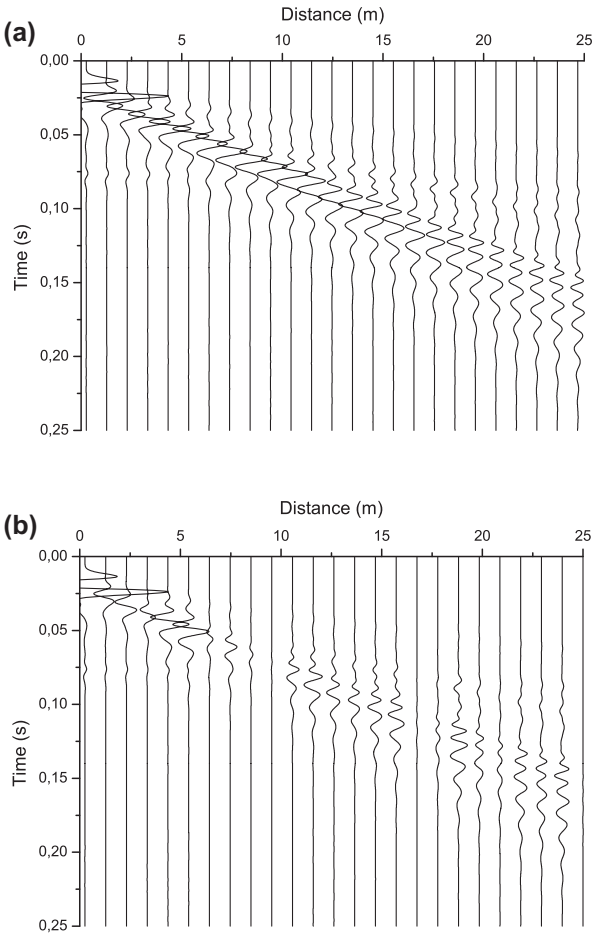

Figure 10 Model 3. Synthetic seismogram acquired with optimal (a) and poor (b) ground-to-geophone transmission.

$\rho = 2000$ kg/m^3, $Q_P = 100$ and $Q_S = 80$. The geophone weight and plate radius are 1 kg and 3 cm, respectively. In this case, the energy transmission from the soil to the geophone is assumed to be $\sqrt{\mathcal{T}}$, where $\mathcal{T}$ is given in equation (32) [$\mathcal{T}(\gamma = 0)$ corresponds to a welded interface or optimal transmission, according to equation (26)]. The transmission coefficient $\mathcal{T}$ at each geophone is obtained by assuming a range of stiffness characteristic b from 40–4000 1/mm, weighted at each geophone by 25 random numbers between 0–1. Figure 10 shows the synthetic seismogram of the vertical particle-velocity component acquired with optimal transmission (no weights) (a) and poor (b) energy transmission. We have to distinguish between geological and non-geological effects. This example holds for a specific soil and given radius and weight of the plate. If the soil changes along the seismic line, the amplitude will change according to the soil (geological) properties. If the effective area of contact changes along the line the amplitude is affected. This fact and changes in the base plate weight are related to non-geological amplitude variations.

CONCLUSIONS

Three models are proposed to estimate the geophone-ground coupling for circular base plates of varying radii and weight. Two existing models, based on the full-wave theory and developed by Wolf and Hoover and O'Brien, predict that the resonant frequency increases with increasing plate radius. A new model introduced in this work considers that the plate-ground contact is based on a boundary condition modelling partial coupling and leading to the damped oscillator equation of motion. The resonant frequency is independent of the geophone weight and plate radius, while the recorded energy increases with increasing weight and decreasing base plate area (as predicted from our own experiments and measurements by Krohn).

The main model parameters describing the coupling and the damped oscillations, i.e., the resonant frequency and damping constant, can be obtained from measurements of peak frequencies and amplitudes. Moreover, we compute geophone signals for different grounds and varying plate radii based on the first model. Since the resonant frequency is independent of the plate weight, the signal is the same for varying weight. Finally, we simulate seismic acquisition with optimal and poor energy transmission from the ground to the geophone, based on the geophone-ground coupling model developed in this work. The examples regard land streamers. In the case of ocean-bottom sensors, the effective weight and mass could be different because of buoyancy.

ACKNOWLEDGEMENTS

This work was funded by KACST and the CO2Monitor project. The authors wish to thank two anonymous reviewers and Christine Krohn for her help in clarifying some of the concepts involved in this work.

REFERENCES

Beaudoin, G. and Reasnor, M. 2010. Atlantis time-lapse ocean bottom node survey: A project team's journey from acquisition through processing. *SEG Expanded Abstracts*, 4155–4158.

Carcione, J.M. 1996. Elastodynamics of a non-ideal interface: Application to crack and fracture scattering. *Journal of Geophysical Research* **101**, 28177–28188.

Carcione, J.M. 1998. Scattering of elastic waves by a plane crack of finite width in a transversely isotropic medium. *International*

Journal of Numerical and Analytical Methods in Geomechanics **22**, 263–275.

Carcione, J.M. 2007. *Wave fields in real media: Wave propagation in anisotropic, anelastic, porous and electromagnetic media*, Handbook of Geophysical Exploration, vol. **38**, Elsevier (2nd edition, revised and extended).

Carcione, J.M. and Picotti, S. 2012. Reflection and transmission coefficients of a fracture in transversely isotropic media. *Studia Geophysica et Geodaetica* **56**, 307–322.

Dimech, J.-L. 2010. Ground coupling tests for better land streamer design. BSc (Geophysics), Report GPH 8/10, Curtin University, November 2010.

Drijkoningen, G., Rademakers, F., Slob, E.C. and Fokkema, J.T. 2006. A new elastic model for ground coupling of geophones with spikes. *Geophysics* **71**, Q9–Q17.

Eiken, O., Degutsch, M., Riste, P. and Rod, K. 1989. Snowstreamer: an efficient tool in seismic acquisition. *First Break* **9**, 374-378.

Fail, J.P., Grau, G. and Lavergne, M. 1962. Couplage des sismographes avec le sol. *Geophysical Prospecting* **10**, 182–147.

Fioravante, V., Ghionna, V.N., Pedroni, S. and Porcino, D. 1999. A constant normal stiffness direct shear box for soil-solid interface tests. *Rivista Italiana di Geotecnica* **3**, 7–22.

Hoover, G.M. and O'Brien, J.T. 1980. The influence of the planted geophone on seismic land data. *Geophysics* **45**, 1239–1253.

Hunt, M.L. and Vriend, N.M. 2010. Booming sand dunes. *Annual Review of Earth and Planetary Sciences* **38**, 281–301.

Jiang, X.-W., Wan, L., Wang, X.-S., Liang, S.-H. and Hub, B.X. 2009. Estimation of fracture normal stiffness using transmissivity-depth correlation. *International Journal of Rock Mechanics and Mining Sciences* **46**, 51–58.

Kosloff, D. and Carcione, J.M. 2010. 2-D simulation of Rayleigh waves with staggered, sine/cosine transforms and variable grid spacing. *Geophysics* **75**, T133–T140.

Krohn, C.E. 1984. Geophone ground coupling. *Geophysics* **49**, 722–731.

Lamer, A. 1970. Couplage sol-geophone. *Geophysical Prospecting* **8**, 300–319.

Miller, B. E., Tsoflias, G. P. and Steeples, D. W. 2009. Automated geophone deployment on pavement for high resolution seismic reflection investigations in support of transportation infrastructure projects. *SEG Expanded Abstracts* 1430–1434.

Moura, R.M. and Senos Matias, M.J. 2012. Geophones on blocks: a prototype towable geophone system for shallow land seismic investigations. *Geophysical Prospecting* **60**, 192–200.

Pilant, W. L. 1979 *Elastic waves in the earth*, Elsevier Science Publishing Co.

Pyrak-Nolte, L.J., Xu, J. and Haley, G.M. 1992. Elastic interface waves along a fracture: Theory and experiment, 33rd U.S. Symposium on Rock Mechanics (USRMS), June 3-5, Santa Fe, NM, USA, 999–1007.

Schoenberg, M. 1980. Elastic wave behavior across linear slip interfaces. *Journal of the Acoustical Society of America* **68**, 1516–1521.

van derVeen, M., Spitzer, R., Green, A.G. and Wild, P. 2001. Design and application of a towed land-streamer system for cost-effective 2-D and pseudo-3-D shallow seismic data acquisition. *Geophysics* **66**, 482–500.

Washburn, H. and Wiley, H. 1941. The effect of the placement of a seismometer in its response characteristics. *Geophysics* **6**, 116–131.

Wolf, A. 1944. The equation of motion of a geophone on the surface of an elastic earth. *Geophysics* **9**, 29–35.

Zangerl, C., Evans, K.F., Eberhardt, E. and Loew, S. 2008. Normal stiffness of fractures in granitic rock: A compilation of laboratory and in-situ experiments. *International Journal of Rock Mechanics and Mining Sciences* **45**, 1500–1507.

APPENDIX

A NEW SOLUTION OF THE HOOVER AND O'BRIEN EQUATION

Rayleigh function (11) has a root at the Rayleigh wavenumber $k = k_R = \omega/v_R$, where v_R is the Rayleigh-wave velocity. $R = 0$ can be re-written as:

$$q^3 - 8q^2 + (24 - 16r^2)q - 16(1 - r^2) = 0, \quad r = v_S/v_P, \qquad q = (v_R/v_S)^2 \tag{A1}$$

(e.g., Carcione 2007), where $v_P = v_2$ and v_S are the P- and S-wave velocities of the ground.

Equation (10) can be written in terms of dimensionless quantities. Let us define:

$$\hat{k} = \frac{k}{k_P} \tag{A2}$$

and the function

$$\begin{aligned} \Phi(\hat{k}) &= \sqrt{\hat{k}^2 - 1}, \hat{k} \geq 1, \\ &= \mathrm{i}\sqrt{1 - \hat{k}^2}, \hat{k} < 1. \end{aligned} \tag{A3}$$

We obtain:

$$\begin{aligned} dk &= r k_S d\hat{k}, \\ k_1 &= r k_S \Phi(\hat{k}), \\ k_2 &= k_S \Phi(r\hat{k}), \\ ka &= p\hat{k}, \\ p &= \omega a/v_P, \end{aligned} \tag{A4}$$

so that:

$$R(k) = k_S^4[(2\hat{k}^2 r^2 - 1)^2 - 4\hat{k}^2 r^3 \Phi(\hat{k})\Phi(r\hat{k})]. \tag{A5}$$

Therefore, equation (10) can be written as:

$$U(E, r, p) = \left[1 + Ap^2 \int_0^\infty \frac{\Phi(\hat{k}) J_1(p\hat{k})}{(2\hat{k}^2 r^2 - 1)^2 - 4\hat{k}^2 r^3 \Phi(\hat{k})\Phi(r\hat{k})} d\hat{k}\right]^{-1}, \tag{A6}$$

where $A = m/(\pi r a^3)$. The properties of the integrand in equation (A6) are such that it is purely imaginary for $\hat{k} \in [0, 1]$, fully complex for $\hat{k} \in [1, 1/r]$ and real for $\hat{k} \in [1/r, \infty]$. Then,

the real part is integrated as $\int_1^{\hat{k}_R}(\cdot)d\hat{k} + \int_{\hat{k}_R}^{\hat{k}_\infty}(\cdot)d\hat{k}$, to deal with the singularity, where $\hat{k}_R = k_R/k_P$ and $\hat{k}_\infty = 200$. The imaginary part is integrated as $\int_0^{1/r}(\cdot)d\hat{k}$, The integrals are solved with high accuracy using Gauss-Chebyshev integration with dense sampling and shifting the singularity by re-writting equation (A3) as:

$$\begin{aligned}\Phi(\hat{k}) &= \sqrt{\hat{k}^2 - (1 - \mathrm{i}\epsilon)}, \hat{k} \geq 1, \\ &= \mathrm{i}\sqrt{(1 - \mathrm{i}\epsilon) - \hat{k}^2}, \hat{k} < 1.\end{aligned} \tag{A7}$$

The value $\epsilon = 10^{-6}$ works very well. Alternatively, the method proposed by Hoover and O'Brien (1980) in their appendix can be used.